British Journal of Anaesthesia **95 (4)**: 538–48 (2005)
doi:10.1093/bja/aei212 Advance Access publication August 26, 2005

BJA

RESPIRATION AND THE AIRWAY

Effects of alveolar dead-space, shunt and $\dot{V}/\dot{Q}$ distribution on respiratory dead-space measurements

Y. Tang, M. J. Turner and A. B. Baker*

Department of Anaesthetics, University of Sydney, Royal Prince Alfred Hospital, Sydney, NSW 2050, Australia

**Corresponding author: Department of Anaesthetics, Royal Prince Alfred Hospital, Building 89 Level 4, Missenden Rd, Camperdown, NSW 2050, Australia. E-mail: bbaker@usyd.edu.au*

Background. Respiratory dead-space is often increased in lung disease. This study evaluates the effects of increased alveolar dead-space ($V_{D_{alv}}$), pulmonary shunt, and abnormal ventilation perfusion ratio ($\dot{V}/\dot{Q}$) distributions on dead-space and alveolar partial pressure of carbon dioxide ($P_{A_{CO_2}}$) calculated by various methods, assesses a recently published non-invasive method (Koulouris method) for the measurement of Bohr dead-space, and evaluates an equation for calculating physiological dead-space ($V_{D_{phys}}$) in the presence of pulmonary shunt.

Methods. Pulmonary shunt, $\dot{V}/\dot{Q}$ distribution and $V_{D_{alv}}$ were varied in a tidally breathing cardiorespiratory model. Respiratory data generated by the model were analysed to calculate dead-spaces by the Fowler, Bohr, Bohr–Enghoff and Koulouris methods. $P_{A_{CO_2}}$ was calculated by the method of Koulouris.

Results. When $V_{D_{alv}}$ is increased, $V_{D_{phys}}$ can be recovered by the Bohr and Bohr–Enghoff equations, but not by the Koulouris method. Shunt increases the calculated Bohr–Enghoff dead-space, but does not affect Fowler, Bohr or Koulouris dead-spaces, or $V_{D_{phys}}$ estimated by the shunt-corrected equation if pulmonary artery catheterization is available. Bohr–Enghoff but not Koulouris or Fowler dead-space increases with increasing severity of $\dot{V}/\dot{Q}$ maldistribution. When alveolar PCO_2 is increased by any mechanism, $P_{A_{CO_2}}$ calculated by Koulouris' method does not agree well with average alveolar PCO_2.

Conclusions. Our studies show that increased pulmonary shunt causes an apparent increase in $V_{D_{phys}}$, and that abnormal $\dot{V}/\dot{Q}$ distributions affect the calculated $V_{D_{phys}}$ and $V_{D_{alv}}$, but not Fowler dead-space. Dead-space and $P_{A_{CO_2}}$ calculated by the Koulouris method do not represent true Bohr dead-space and $P_{A_{CO_2}}$ respectively, but the shunt-corrected equation performs well.

Br J Anaesth 2005; **95**: 538–48

Keywords: computers; lung, shunting; ventilation, deadspace; ventilation, ventilation–perfusion

Symbols used in the paper

$P_{A_{CO_2}}$=ideal alveolar carbon dioxide partial pressure; Pa_{CO_2}=arterial carbon dioxide partial pressure; $P_{A_{KCO_2}}$=$P_{A_{CO_2}}$ calculated by Koulouris method; $P_{A_{XCO_2}}$=volume-weighted average of PCO_2 in all the alveolar compartments in the model; $P_{E_{CO_2}}$=mixed expired carbon dioxide partial pressure; $P_{E'_{CO_2}}$=end-tidal partial pressure of carbon dioxide; $\dot{Q}_s/\dot{Q}$=pulmonary shunt fraction; $V_{D_{alv}}$=alveolar dead-space; $V_{D_{anat}}$=anatomical dead-space in the model; $V_{D_{BE}}$=Bohr–Enghoff dead-space calculated by substituting Pa_{CO_2} for $P_{A_{CO_2}}$ in Bohr equation; $V_{D_{Bohr}}$=Bohr dead-space; $V_{D_{corr}}$=Bohr–Enghoff dead-space corrected for shunt; $V_{D_{ET}}$=dead-space calculated by substituting $P_{E'_{CO_2}}$ for $P_{A_{CO_2}}$ in Bohr equation; $V_{D_{Fowler}}$=Fowler dead-space; V_{D_K}=dead-space calculated by Koulouris method; $V_{D_{phys}}$=physiological dead-space (total dead-space in the model); $\dot{V}/\dot{Q}$=ventilation to perfusion ratio; V_T=tidal volume; $V_{T_{alv}}$=alveolar tidal volume (V_T–$V_{D_{Fowler}}$).

Introduction

Respiratory dead-space measurements have been used in determining surfactant efficacy in surfactant-depleted lungs,[1] diagnosing pulmonary embolism,[2 3] providing useful prognostic information early in the course of acute respiratory distress syndrome,[4] predicting successful extubation

in infants and children,[5] and separating patients with asthma from patients with emphysema with the same degree of airways obstruction.[6] All these clinical applications depend on accurate measurements of respiratory dead-space.

Bohr[7] dead-space ($V_{D_{Bohr}}$) is a function of ideal alveolar partial pressure of carbon dioxide ($P_{A_{CO_2}}$). Because $P_{A_{CO_2}}$ is difficult to estimate, Enghoff[8] substituted arterial partial pressure of carbon dioxide ($P_{a_{CO_2}}$) for $P_{A_{CO_2}}$, giving rise to the Bohr–Enghoff dead-space (Appendix A), usually referred to as physiological dead-space ($V_{D_{phys}}$). Alveolar dead-space[9] is commonly defined as the difference between $V_{D_{phys}}$ and the anatomical dead-space ($V_{D_{Fowler}}$), which is estimated by a method proposed by Fowler[10] (Appendix A). Disadvantages of the Bohr–Enghoff method are that it is invasive and cannot be used breath-by-breath when $P_{a_{CO_2}}$ is changing rapidly. Recently, Koulouris and colleagues[11] reported a new non-invasive method to calculate Bohr dead-space and $P_{A_{CO_2}}$ based on an analysis of the expired carbon dioxide volume *vs* expired tidal volume curve from a single expiration (Appendix A). This technique is apparently simple and non-invasive, but has not been validated independently.

Shunt reduces the overall efficiency of gas exchange and results in arterial blood gas tensions closer to those of mixed venous blood, thus increasing the measured apparent physiological dead-space by increasing $P_{a_{CO_2}}$.[12] A method for correcting dead-space measurements for the effects of shunt has been reported by Kuwabara and Duncalf[13] (Appendix A) but its validity has not been demonstrated.

Inhomogeneity of ventilation/perfusion ($\dot{V}/\dot{Q}$) ratio increases the measured alveolar dead-space by two mechanisms. Firstly, the venous admixture is increased from lung regions with low $\dot{V}/\dot{Q}$ ratio; secondly, lung units with high $\dot{V}/\dot{Q}$ ratio contribute to physiological dead-space.

Although series dead-space can be altered easily in studies *in vivo*, it is difficult to control changes in alveolar dead-space and the $\dot{V}/\dot{Q}$ distribution. Thus the effects of changes in $\dot{V}/\dot{Q}$ distribution on measures of respiratory dead-space have not been studied systematically.

The aims of this study were to assess the method of Koulouris and colleagues[11] for calculating Bohr dead-space and alveolar P_{CO_2}, to demonstrate the validity of the correction proposed by Kuwabara and Duncalf[13] for calculating physiological dead-space in the presence of pulmonary shunt, and to evaluate the effects of varying alveolar dead-space, pulmonary shunt and abnormal $\dot{V}/\dot{Q}$ distributions on $P_{A_{CO_2}}$ and dead-space calculated by five different methods.[7 8 10 11 13]

Methods

The computer model

We used a comprehensive, mathematical, tidally breathing computer model of the cardiorespiratory system.[14] The model incorporates a 15-compartment approximation to Weibel's lung model A[15] and simulates diffusive and convective transport and storage of gases in the lungs. The branching airways comprise 11 anatomical dead-space compartments and terminate in one unperfused and three perfused alveolar compartments (Fig. 1). Carbon dioxide is stored in two lung tissue compartments.[16] Ventilation and $\dot{V}/\dot{Q}$ heterogeneity can be simulated by varying the inspired gas distribution and the fraction of the cardiac output perfusing the three perfused alveolar compartments. A variable right-to-left shunt is provided. The model simulates alveolar-capillary diffusion; intraventricular and intravascular mixing; variable transport delays; intravascular storage; and carbon dioxide and oxygen storage, production and consumption in eight anatomically appropriate body compartments. Molar quantities of oxygen, nitrogen and carbon dioxide are conserved in the model. Non-linear blood gas dissociation curves[17] include the Haldane and Bohr effects. The tissue dissociation curves are after Farhi and Rahn[18] and Cherniack and Longobardo.[19] The respiratory flow waveform was selected to match a mechanically ventilated subject: constant inspiratory flow followed by exponential expiratory flow. The model is implemented in Matlab and Simulink (Mathworks, Natick, MA, USA) and has been verified against published human data.[14] Additional validation is described in Appendix B.

Part 1. Effect of the ratio of physiological dead-space to tidal volume on respiratory dead-space measurements

The model was configured to simulate a 70 kg healthy adult male subject with respiratory parameters, as shown in Table 1. The ratio of the tidal volume that reaches alveolar dead-space (Alv DS in Fig. 1) to the alveolar tidal volume was set in turn to 1, 10, 20, 30, 40 and 50%. Alveolar tidal volume ($V_{T_{alv}}$) is the volume of fresh inspired gas that reaches the alveoli. Corresponding ratios of physiological dead-space to tidal volume in the model were 30, 36, 43, 51, 58 and 65%, respectively. The $\dot{V}/\dot{Q}$ ratios in the three ventilated and perfused lung compartments were the same, and decreased as the dead-space increased. Total anatomical dead-space and total alveolar volume were kept constant. The volumes of the alveolar dead-space compartment and the associated anatomical dead-space compartments in the model were increased in proportion to the alveolar dead-space ventilation. The volumes of the perfused alveoli and their associated anatomical dead-space compartments were decreased in proportion to the decreasing ventilation directed to those alveoli. Under each condition, the model was run for 7200 s simulation time to achieve steady-state P_{CO_2} and P_{O_2} in mixed venous blood, and alveolar and body compartments. The data were sampled at 100 Hz and stored for off-line analysis. The last complete respiratory cycle in each 2-h run was analysed. The simulated subject was assumed to be anaesthetized and paralysed and $P_{a_{CO_2}}$ was allowed to reach unphysiological levels.

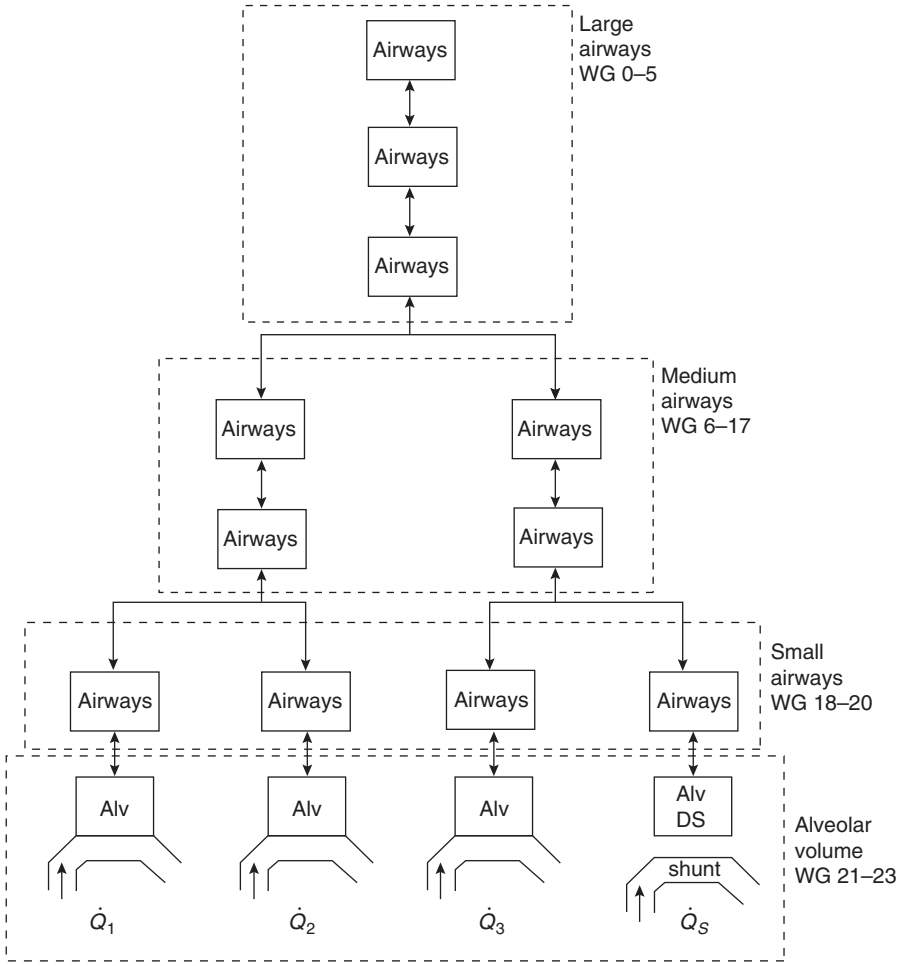

Fig 1 Block diagram of the airway and alveolar compartments in the comprehensive cardiorespiratory system model. The respiratory system incorporates a 15-compartment approximation to Weibel's lung model. WG=Weibel generations; Alv=alveolar; DS=dead-space.

Table 1 Model parameters

Respiratory parameters	Value	Unit
Tidal volume	0.75	litre
Respiratory rate	10	bpm
I:E ratio	1:2.3	–
Airway temperature	35	°C
FRC	2.2	litre
$F_{I_{O_2}}$	35	%
Instrument dead-space	50	ml
Airway dead-space	170	ml
Pulmonary shunt	2	%
Cardiac output	5.29	litre min^{-1}
Hb	15	g dl^{-1}

Part 2. Effect of pulmonary shunt on respiratory dead-space measurements

In this part of the study the ratio of alveolar dead-space to alveolar tidal volume was kept constant at 1%, corresponding to a ratio of physiological dead-space to tidal volume of 30%. The tidal volume in the alveolar dead-space was 5.3 ml. The pulmonary shunt was set in turn to 2, 10, 20, 30, 40 and 50% of the total pulmonary blood flow and the other respiratory parameters were the same as in Part 1 (Table 1). $\dot{V}/\dot{Q}$ ratios of all the perfused compartments were the same, and increased as the shunt increased. Under each condition the model was run for 7200 s of simulation time to reach steady state P_{CO_2} and P_{O_2}. Data from the last complete respiratory cycle in each 2-h run were recorded and analysed.

Part 3. Effect of $\dot{V}/\dot{Q}$ ratio heterogeneity on respiratory dead-space measurements

The ratio of alveolar dead-space to alveolar tidal volume and the pulmonary shunt were set to 1% and 2% respectively. The minute alveolar ventilation of 5.30 litre min^{-1} and the pulmonary perfusion of 5.40 litre min^{-1} were unevenly distributed to the three ventilated and perfused alveolar compartments to create $\dot{V}/\dot{Q}$ values of 0.1, 1.0 and 10 to simulate patients with chronic obstructive pulmonary disease.[20] The percentage perfusion to the middle $\dot{V}/\dot{Q}$ compartment ($\dot{V}/\dot{Q}$=1) was set in turn to 98, 78, 58, 38

and 18% of pulmonary blood flow to simulate increasing severity of $\dot{V}/\dot{Q}$ mismatch, and the ventilation and perfusion of all three ventilated and perfused compartments were calculated by the method described in Appendix C. The model was run for 7200 s simulation time at each setting to reach steady-state P_{CO_2} and P_{O_2} in mixed venous blood and alveolar and body compartments, and the respiratory parameters were measured and analysed. Log standard deviations of the perfusion distributions were calculated for each condition.

Data analysis

Pa_{CO_2} fluctuated during respiration and was therefore averaged over a complete respiratory cycle. $P_{A_{CO_2}}$ is the volume-weighted average of the P_{CO_2} in the three perfused and ventilated alveolar compartments averaged over one respiratory cycle in Parts 1 and 2 of this study. $P_{A_{XCO_2}}$ is the volume-weighted average of the P_{CO_2} in all the alveolar compartments, including the alveolar dead-space compartment, averaged over one respiratory cycle. $V_{D_{Fowler}}$ was calculated by the equal area method (Appendix A).[10 21 22] $V_{D_{Bohr}}$ (Parts 1 and 2 of this study) and $V_{D_{BE}}$ (Parts 1, 2 and 3 of this study) were calculated according to Equations 1 and 2 (Appendix A) respectively. Bohr–Enghoff dead-space corrected for the effects of shunt ($V_{D_{Corr}}$) was calculated using Equation 3 (Appendix A). The calculation of Bohr dead-space by the method of Koulouris and colleagues[11] (V_{D_K}) is described in Appendix A. An estimate of the Bohr dead-space was also calculated by substituting end-tidal carbon dioxide partial pressure ($P_{E'_{CO_2}}$) for $P_{A_{CO_2}}$ (Equation 4, Appendix A). We refer to this dead-space as $V_{D_{ET}}$. The physiological dead-space of the model ($V_{D_{phys}}$) was calculated as follows:

$$V_{D_{phys}} = V_{D_{anat}} + (V_T - V_{D_{anat}})F_{D_{alv}}$$

where $V_{D_{anat}}$ is the volume of the anatomical dead-space compartments in the model and $F_{D_{alv}}$ is the fraction of the tidal volume that enters the parallel dead-space compartment.

Table 2 $\dot{V}/\dot{Q}$ ratios of perfused alveolar compartments and steady state arterial blood gas tensions in parts 1 and 2 of this study. $\dot{V}/\dot{Q}$ is the ventilation to perfusion ratio for the three ventilated and perfused compartments with equal $\dot{V}/\dot{Q}$

$V_{D_{alv}}/V_{T_{alv}}$	1%	10%	20%	30%	40%	50%
$\dot{V}/\dot{Q}$	0.95	0.87	0.77	0.67	0.58	0.48
Pa_{CO_2} (kPa)	4.7	5.1	5.6	6.2	7.0	8.1
Pa_{O_2} (kPa)	23.1	23.4	22.9	22.2	21.2	19.9
Shunt	**2%**	**10%**	**20%**	**30%**	**40%**	**50%**
$\dot{V}/\dot{Q}$	0.95	0.88	0.78	0.68	0.58	0.49
Pa_{CO_2} (kPa)	4.7	4.8	4.9	5.0	5.1	5.4
Pa_{O_2} (kPa)	23.9	17.1	13.0	10.2	8.1	6.5

Results

Part 1. Effect of the ratio of physiological dead-space to tidal volume on respiratory dead-space measurements

The $\dot{V}/\dot{Q}$ ratios in the three ventilated and perfused alveolar compartments and the arterial partial pressures of carbon dioxide and oxygen resulting from increased alveolar dead-space are shown in Table 2. Increased alveolar dead-space affects Pa_{CO_2} more than Pa_{O_2}. Figure 2A shows simulated and calculated P_{CO_2} as functions of the ratio of physiological dead-space to tidal volume. Pa_{CO_2} and $P_{A_{CO_2}}$, predicted by the model, do not differ greatly and increase monotonically with increasing physiological dead-space fraction. $P_{A_{XCO_2}}$ and the associated measured values ($P_{E'_{CO_2}}$ and $P_{A_{KCO_2}}$) decrease slightly with increasing physiological dead-space. The maximum difference between $P_{E'_{CO_2}}$, $P_{A_{XCO_2}}$

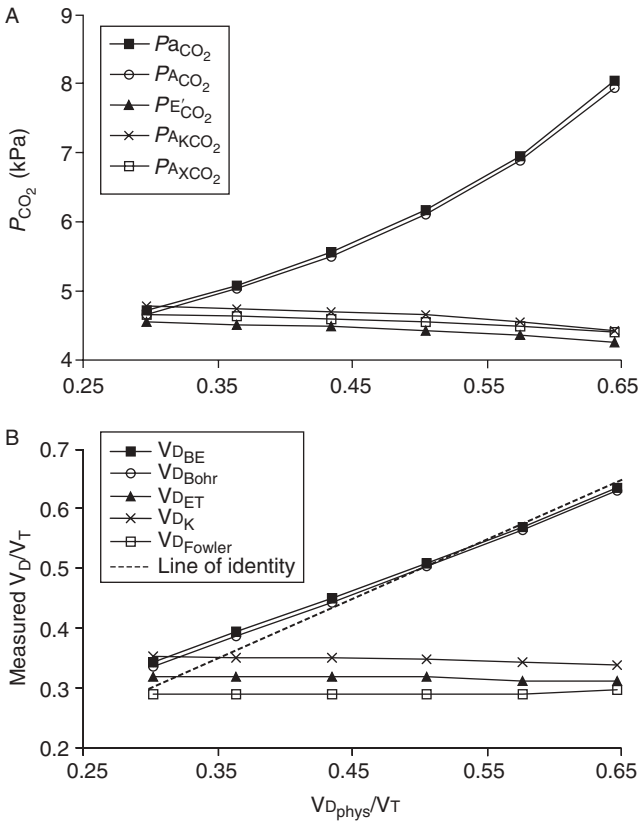

Fig 2 (A) Carbon dioxide partial pressures and (B) measured ratios of dead-space volumes to tidal volume as functions of $V_{D_{phys}}/V_T$ (model physiological dead-space to tidal volume ratio). $P_{A_{CO_2}}$ is arterial P_{CO_2} predicted by the model. $P_{A_{CO_2}}$ is volume and time-averaged P_{CO_2} in the perfused alveoli of the model. $P_{A_{XCO_2}}$ is volume and time-averaged P_{CO_2} in all the alveoli of the model. $P_{E'_{CO_2}}$ is end-tidal P_{CO_2}. $P_{A_{KCO_2}}$ is alveolar P_{CO_2} calculated by Koulouris' method (Appendix A). $V_{D_{BE}}$ is Bohr–Enghoff dead-space calculated by using Appendix Equation 2. $V_{D_{Bohr}}$ is Bohr dead-space calculated by using Equation 1. $V_{D_{ET}}$: dead-space calculated by using Equation 4. V_{D_K} is dead-space calculated by Koulouris' method (Appendix A). $V_{D_{Fowler}}$ is anatomical dead-space calculated by Fowler's graphic method. Dashed straight line in B is the line of identity.

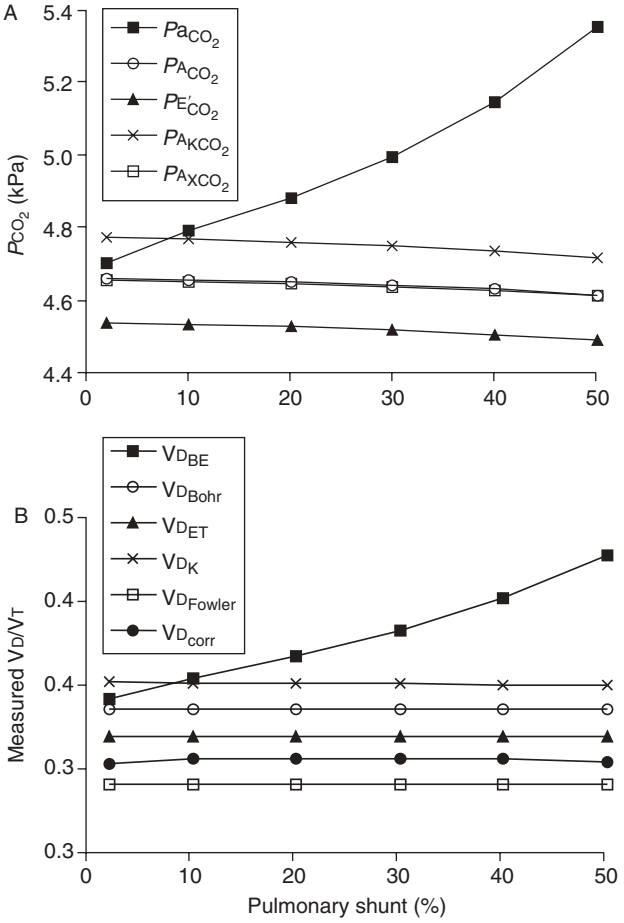

Fig 3 (A) Carbon dioxide partial pressures and (B) measured dead-spaces as functions of pulmonary shunt. Abbreviations are the same as in Fig. 2. $V_{D_{corr}}$ is the Bohr–Enghoff dead-space corrected by the Kuwabara and Duncalf[13] equation in the presence of right-to-left shunt (Appendix Equation 3).

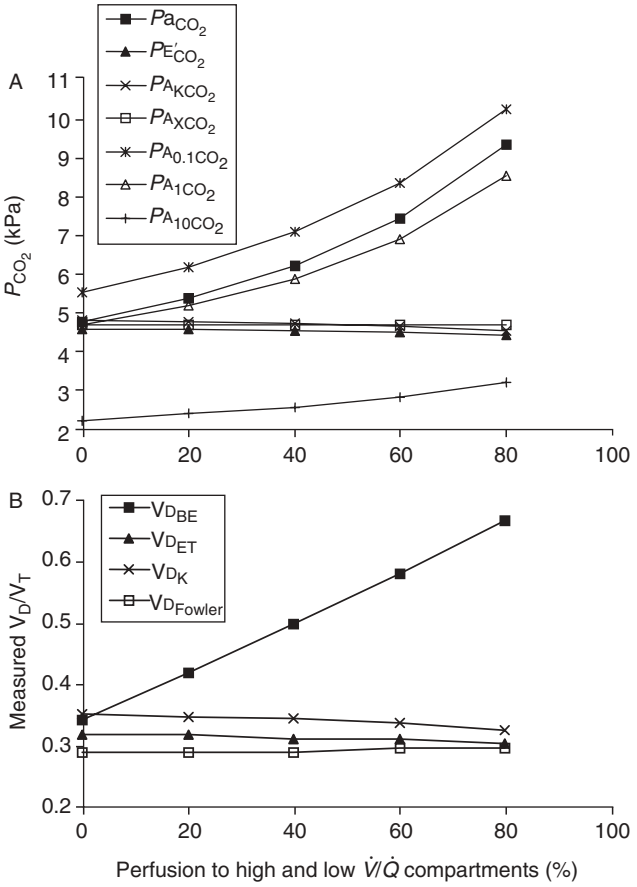

Fig 4 (A) Carbon dioxide partial pressures and (B) measured dead-spaces as functions of the combined pulmonary perfusion of the high and low $\dot{V}/\dot{Q}$ compartments. $Pa_{0.1CO_2}$, Pa_{1CO_2} and Pa_{10CO_2} are PCO_2 in the low $\dot{V}/\dot{Q}$, middle $\dot{V}/\dot{Q}$ and high $\dot{V}/\dot{Q}$ compartments respectively. Other abbreviations as in Fig. 2.

and PA_{KCO_2} is less than 0.25 kPa (2 mmHg) under all conditions studied.

Figure 2B shows calculated dead-space to tidal volume ratios as functions of true physiological dead-space to tidal volume ratio. VD_{Bohr} and VD_{BE} increase with increasing physiological dead-space. Both VD_{Bohr} and VD_{BE} overestimate the model physiological dead-space when alveolar dead-space is small but slightly underestimate physiological dead-space when the model alveolar dead-space is large. VD_K, VD_{Fowler} and VD_{ET} are approximately independent of alveolar dead-space, shunt and $\dot{V}/\dot{Q}$ ratio heterogeneity and lie between approximately 29 and 35% under all conditions studied (Figs 2–4).

Part 2. Effect of pulmonary shunt on respiratory dead-space measurements

The ventilation and perfusion to the three ventilated and perfused alveolar compartments and the arterial partial pressure of carbon dioxide and oxygen when the shunt is increased are shown in Table 2. Shunt affects Pa_{O_2} more than Pa_{CO_2}. Pa_{CO_2} increases with increasing pulmonary shunt, while PE'_{CO_2}, PA_{KCO_2} and the volume-averaged PA_{CO_2} and PA_{XCO_2} fall slightly (Fig. 3A). The effect of pulmonary shunt on the partial pressure of carbon dioxide in the alveoli and in the arterial blood is less marked than the effect of directing similar proportions of tidal volume to alveolar dead-space.

The Bohr–Enghoff dead-space increases with increasing pulmonary shunt (Fig. 3B). VD_{Corr} and VD_{Bohr} are greater than VD_{Fowler} but smaller than VD_K and are approximately independent of shunt.

Part 3. Effect of $\dot{V}/\dot{Q}$ ratio heterogeneity on respiratory dead-space measurements

The perfusion and ventilation of each compartment, the respiratory variables and the arterial partial pressures of carbon dioxide and oxygen are shown in Table 3. In the $\dot{V}/\dot{Q}$ ratio heterogeneity study it was not appropriate to calculate Bohr dead-space due to the variation of PCO_2 among the ventilated and perfused alveoli. Pa_{CO_2} and the PCO_2 in each individual alveolar compartment increase with increasing heterogeneity of the $\dot{V}/\dot{Q}$ ratio (Fig. 4A).

Table 3 Ventilation and perfusion parameters of perfused alveolar compartments in Part 3 of this study

Perfusion to high and low $\dot{V}/\dot{Q}$ compartments (%)	Pa_{O_2} (kPa)	Pa_{CO_2} (kPa)	Log SD $\dot{Q}$	High: $\dot{V}/\dot{Q}$=10		Middle: $\dot{V}/\dot{Q}$=1.0		Low: $\dot{V}/\dot{Q}$=0.1	
				Ventilation (litre min^{-1})	Perfusion (litre min^{-1})	Ventilation (litre min^{-1})	Perfusion (litre min^{-1})	Ventilation (litre min^{-1})	Perfusion (litre min^{-1})
0	23.9	4.7	0.012	0.0080	0.0008	5.27	5.29	7.7e−7	7.7e−6
20	14.8	5.4	0.42	0.99	0.099	4.21	4.21	0.098	0.98
40	10.9	6.2	0.54	1.97	0.20	3.13	3.13	0.20	1.96
60	8.6	7.4	0.60	2.95	0.30	2.05	2.05	0.29	2.94
80	6.6	9.2	0.61	3.93	0.39	0.97	0.97	0.39	3.92

The P_{CO_2} of each alveolar compartment is inversely related to the $\dot{V}/\dot{Q}$ ratio of the compartment. The $V_{D_{BE}}/V_T$ ratio increases from 30.5% at optimal $\dot{V}/\dot{Q}$ distribution to 64.9% when 78% of the pulmonary perfusion is distributed to the compartments with $\dot{V}/\dot{Q}$ of 0.1 and 10 (Fig. 4B).

Discussion

This study found that the Kouloumis method for calculating Bohr dead-space overestimates slightly when alveolar dead-space is small but substantially underestimates Bohr dead-space when alveolar dead-space is increased. V_{D_K} appears to be no better than $V_{D_{ET}}$ as an estimate of Bohr dead-space under the conditions in this study. The Kouloumis method for calculating alveolar P_{CO_2} does not respond to changes in the P_{CO_2} of ventilated and perfused alveoli caused by increasing alveolar dead-space. As respiratory dead-space has been widely studied and used in anaesthesia and in emergency and intensive care medicine, it is important that new methods for dead-space measurement should be validated independently before they are used clinically. Bohr dead-space as calculated by the Kouloumis method is not accurate and thus the Kouloumis method is not validated by this study.

Pulmonary embolism results in lung units that are poorly perfused but maintain approximately normal ventilation.[23] Although pulmonary embolism is a complex pathological entity with mixed presentation of shunt and dead-space, the increased pulmonary dead-space in Part 1 of this study approximately simulates the main features of gas exchange in patients with pulmonary embolism. The Bohr–Enghoff dead-space accurately follows the increase in the model alveolar dead-space, while the Fowler dead-space is unaffected (Fig. 2B). Hence, calculated alveolar dead-space, one of the diagnostic markers of pulmonary embolism,[23] increases. Dead-space calculated by the Kouloumis method does not correlate well with alveolar dead-space or Bohr dead-space, suggesting that the Kouloumis method cannot contribute to the diagnosis of pulmonary embolism.

Pulmonary shunt increases $V_{D_{BE}}$ but does not affect $V_{D_{Fowler}}$ or $V_{D_{Bohr}}$. The equation of Kuwabara and Duncalf[13] (Equation 3, Appendix A) calculates model dead-space correctly in the presence of substantial shunt. Use of this correction equation requires pulmonary artery catheterization due to the need for measurement of shunt, mixed venous P_{CO_2} and Pa_{CO_2}.

The invalidity of the Kouloumis method can be demonstrated theoretically. The Bohr dead-space equation (Equation 1, Appendix A) assumes that expired gas emanates from two compartments: a perfused alveolar compartment and an unperfused dead-space. The Bohr equation makes no assumptions regarding the sequence in which gas from the two compartments is expired. In contrast, the Kouloumis method (Fig. A1B in Appendix A) assumes that an expiration comprises two sequential volumes: a dead-space (V_{D_K}=*ia*) containing a volume of carbon dioxide [V_{CO_2}(d)=*ay*] is expired first at a mean carbon dioxide concentration of Fd=*ya/ia*, and the remaining carbon dioxide (*ce′*) is assumed to be expired in a subsequent volume *ae* of alveolar gas at end-tidal carbon dioxide concentration $F_{E'_{CO_2}}$=*ce′/ae*=*ya/da*. In Figure A1B in Appendix A the lines *ia* and *id* represent V_{D_K} and $V_{D_{ET}}$ respectively. Hence the line *da*, which represents the difference between V_{D_K} and $V_{D_{ET}}$, can be expressed as $V_{CO_2}(d)/F_{E'_{CO_2}}$. V_{D_K} and $V_{D_{ET}}$ are therefore related by:

$$V_{D_K}=V_{D_{ET}}+V_{CO_2}(d)/F_{E'_{CO_2}}$$

where V_{CO_2}(d) is the volume of carbon dioxide expired in V_{D_K}. Similarly, it can be shown that $P_{A_{KCO_2}}$ and $P_{E'_{CO_2}}$ are related by:

$$P_{A_{KCO_2}}/P_{E'_{CO_2}}=V_{CO_2}/(V_{CO_2}-V_{CO_2}(d))$$

where V_{CO_2} is the total amount of carbon dioxide expired in one breath. It can be concluded that V_{D_K} and $P_{A_{KCO_2}}$ are always larger than $V_{D_{ET}}$ and $P_{E'_{CO_2}}$ respectively.

Alveolar P_{CO_2} increases during expiration and reaches a peak shortly after end-expiration. *In vivo*, $P_{E'_{CO_2}}$ is dominated by end-expiratory alveolar gas and can be greater than $P_{A_{CO_2}}$, particularly during exercise or when tidal volumes are large.[24–26] Fletcher and colleagues[27] found zero or negative arterial-to-end-tidal P_{CO_2} differences in 12% of non-pregnant patients during anaesthesia in which large tidal volumes and low respiratory rates were used. In the method of Kouloumis and colleagues,[11] the relationship between V_{D_K} and $V_{D_{ET}}$ is fixed and independent of tidal volume, respiratory rate and alveolar dead-space, so end-tidal P_{CO_2} can never exceed $P_{A_{CO_2}}$.

In this study the simulated subject was assumed to be anaesthetized and paralysed and Pa_{CO_2} was allowed to rise as high as 8.1 and 9.2 kPa when alveolar dead-space and $\dot{V}/\dot{Q}$ ratio heterogeneity respectively were increased. In a study of COPD patients with severe $\dot{V}/\dot{Q}$ heterogeneity, Conti and colleagues[28] reported Pa_{CO_2} values as high as 11.6 kPa in mechanically ventilated patients. Breen and colleagues[29] studied the effects of large pulmonary embolism on carbon dioxide kinetics and physiological dead-space. They found that after 70 min of occlusion of a large pulmonary artery, the Pa_{CO_2} increased from 5.5 to 7.3 kPa and $P_{E'CO_2}$ decreased by 13% of baseline value while physiological dead-space increased from 31 to 52%. Our simulation results are consistent with the *in vivo* observations of Conti and colleagues[28] and Breen and colleagues.[29]

We used a mathematical model for this study to facilitate the controlled variation of alveolar dead-space, anatomical dead-space, pulmonary shunt and $\dot{V}/\dot{Q}$ ratio distribution, which are difficult to change prospectively in *in vivo* studies. A computer model study also avoids the confounding effects associated with biological variations and measurement errors. The main limitations of our computer model include the lumped approximation of the respiratory tree and alveoli, the approximations used to estimate diffusion and convection in the airways and the assumption of equal respiratory time constants and consequent simultaneous emptying of alveolar compartments. The model does not automatically redistribute ventilation or perfusion when these parameters are perturbed and does not simulate hypoxic pulmonary vasoconstriction. These approximations and limitations may affect the shape of the expirogram and hence the calculated dead-space and PCO_2 values. We expect, however, that the limitations of the model affect only the magnitude of the results, not their form or direction.

In conclusion, our simulation results suggest that while the physiological dead-space is estimated well by the Bohr–Enghoff equation when alveolar dead-space and $\dot{V}/\dot{Q}$ ratio distribution vary, respiratory dead-space and alveolar carbon dioxide partial pressure calculated by the Koulouris method do not represent the true Bohr dead-space or alveolar carbon dioxide partial pressure. Increasing pulmonary shunt can cause an apparent increase in $V_{D_{phys}}$, and abnormal $\dot{V}/\dot{Q}$ distributions affect calculated $V_{D_{phys}}$ and $V_{D_{alv}}$, but not Fowler dead-space. The equation suggested by Kuwabara and Duncalf[13] for the calculation of dead-space in the presence of shunt performs well, but requires invasive measurements.

Acknowledgements

The authors are pleased to acknowledge the financial support of an Australian Research Council 'Strategic Partnership with Industry—Research and Training' (ARC-SPIRT) grant, Dräger Australia Pty Ltd, The Joseph Fellowship, The University of Sydney and the Australian National Health and Medical Research Council (NHMRC).

Appendix A. Dead-space calculation methods and symbols

Fowler dead-space

On an expired carbon dioxide concentration *vs* expired volume curve (Fig. A1A), a straight line is fitted to the alveolar plateau between 60 and 90% of expired volume by linear regression.[6] A vertical line is drawn from the regression line to the *x*-axis to divide the rapidly rising part of the carbon dioxide expirogram into two equal areas (p' and q'). The intersection of the perpendicular line and the *x*-axis is the anatomical or Fowler dead-space.[10 22]

Bohr dead-space

Bohr dead-space ($V_{D_{Bohr}}$) is the dead-space calculated by the original Bohr equation:[7 21]

$$V_{D_{Bohr}} = V_T(1-(P_{E_{CO_2}}/P_{A_{CO_2}})) \quad (1)$$

Where $P_{E_{CO_2}}$ is the mixed expired carbon dioxide partial pressure and $P_{A_{CO_2}}$ is the ideal alveolar carbon dioxide partial pressure. In Parts 1 and 2 of this study, $P_{A_{CO_2}}$ is the volume-weighted average of the PCO_2 in the three perfused and ventilated alveolar compartments averaged over one respiratory cycle.

Bohr–Enghoff dead-space

Because of the controversy concerning the definition and estimation of $P_{A_{CO_2}}$,[21] Enghoff[8] suggested substituting Pa_{CO_2} for $P_{A_{CO_2}}$ in the Bohr equation. The dead-space so calculated is termed the Bohr–Enghoff dead-space ($V_{D_{BE}}$):

$$V_{D_{BE}} = V_T(1-(P_{E_{CO_2}}/Pa_{CO_2})) \quad (2)$$

Shunt correction method

In the presence of right-to-left shunt, venous blood mixes with pulmonary capillary blood and raises Pa_{CO_2}, thus increasing the difference between $P_{E_{CO_2}}$ and Pa_{CO_2}. Hence the Bohr–Enghoff dead-space calculated by Equation 2 is increased. Kuwabara and Duncalf[13] applied simple mass balance principles and derived an equation to estimate a corrected physiological dead-space ($V_{D_{corr}}$) in the presence of right-to-left shunt.

$$V_{D_{corr}}/V_T = 1-P_{E_{CO_2}}/(P_{V_{CO_2}}-(P_{V_{CO_2}}-Pa_{CO_2})/(1-\dot{Q}_S/\dot{Q}_T)) \quad (3)$$

where $\dot{Q}_S/\dot{Q}_T$ is the shunt fraction, and $PvCO_2$ is the mixed venous PCO_2.

$V_{D_{ET}}$

Dead-space calculated by using $P_{E'_{CO_2}}$ in place of $P_{A_{CO_2}}$ in the Bohr equation (Equation 1) is termed $V_{D_{ET}}$ in this paper:

$$V_{D_{ET}} = V_T(1-(P_{E_{CO_2}}/P_{E'_{CO_2}})) \quad (4)$$

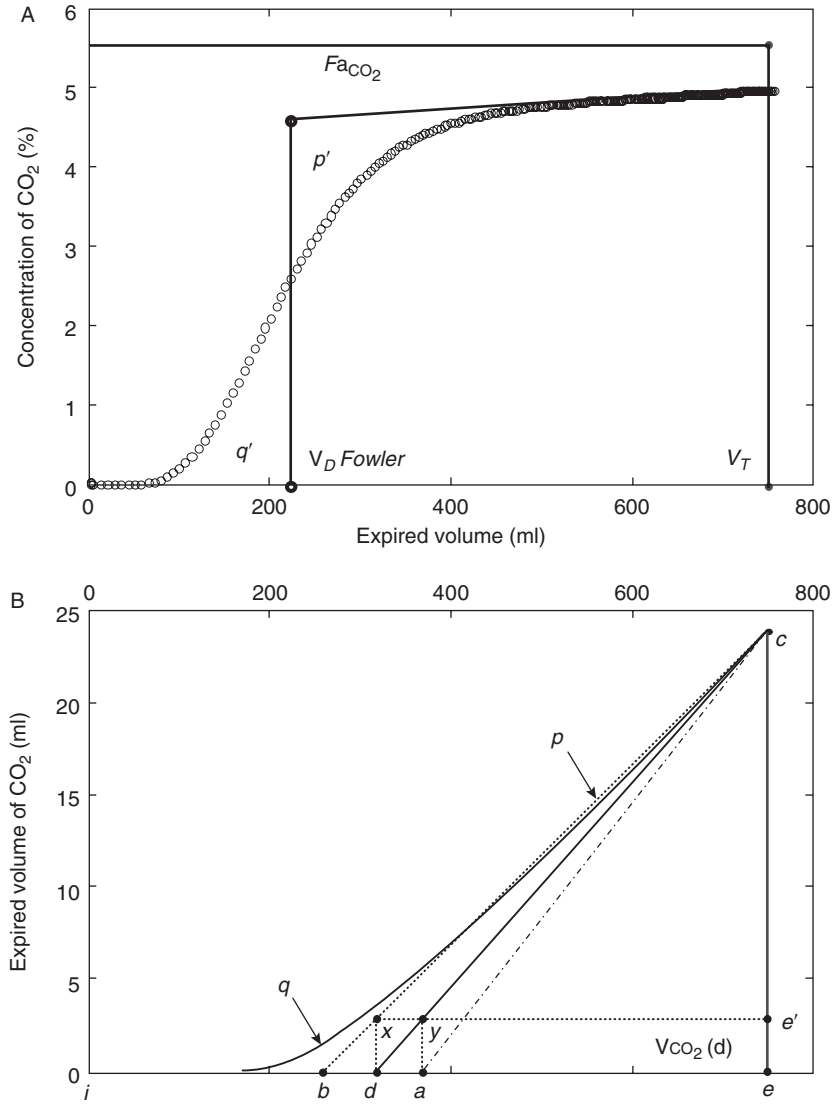

Fig A1 Diagrammatic representations of the Fowler method for calculating anatomical dead-space and the method of Koulouris and colleagues[11] for the calculation of respiratory dead-space and alveolar partial pressure of carbon dioxide$_2$. (A) Expired carbon dioxide concentration as a function of expired volume. Areas p' and q' are equal and the perpendicular line intersects the x-axis at the Fowler dead-space. (B) Expired carbon dioxide volume as a function of expired volume. Areas p and q are equal. According to Koulouris and colleagues,[11] the slope of line ca is an estimate of alveolar carbon dioxide concentration and the lengths ia and ae are estimates of Bohr dead-space and alveolar volume respectively.

Koulouris dead-space

Figure A1B shows expired carbon dioxide volume *vs* expired volume. Line *cb* is drawn such that areas *p* and *q* are equal. Point *d* is chosen such that the slope of line *cd* is end-tidal concentration. The volume *de* is the volume the expired carbon dioxide would occupy at end-tidal carbon dioxide concentration (total volume of carbon dioxide divided by end-tidal carbon dioxide concentration), hence *id* represents $V_{D_{ET}}$ as calculated by Equation 3 above. Line *dx* is perpendicular and intersects *cb* at *x*. Line *xy* is parallel to the *x*-axis and intersects *cd* at *y*. Line *ya* is perpendicular and intersects the *x*-axis at *a*. According to Koulouris and colleagues,[11] lines ee' and $e'c$ represent the quantities of carbon dioxide expired in the dead-space and alveolar gas respectively. The line *ae* represents alveolar tidal volume, line *ia* represents Bohr dead-space and the slope of line *ac* is the alveolar concentration of carbon dioxide.

Appendix B. Validation of the cardiorespiratory model

The model was validated in a clinical study and by comparison of predicted P_{CO_2} with published measurements.

Figure A2A shows the realistic airway, arterial, alveolar and mixed venous P_{CO_2} changes with time in the tidally breathing model. The model simulated a 70-kg male subject who was mechanically ventilated with a tidal volume of 9 ml kg^{-1} at a respiratory rate of 10 bpm. Other parameters

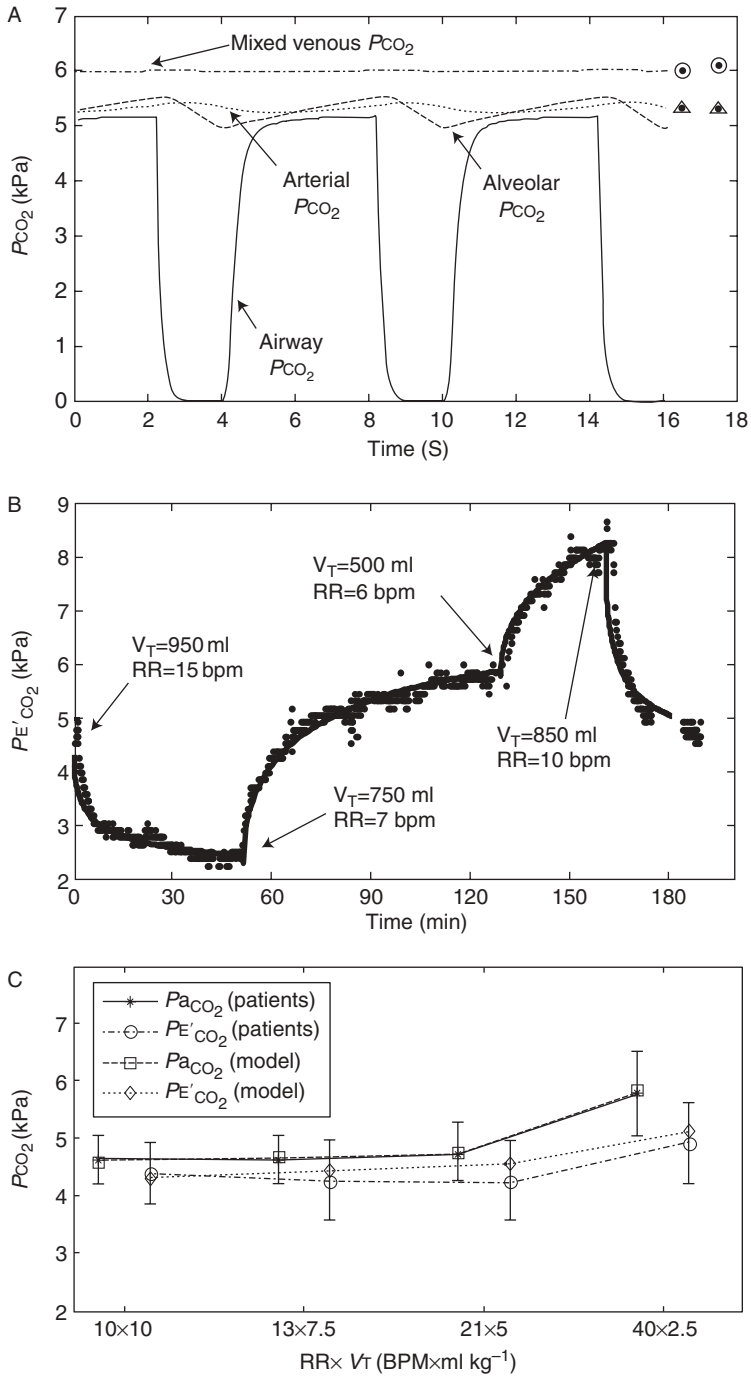

Fig A2 Validation of the computer model. (A) Simulation of airway, arterial, alveolar and mixed venous P_{CO_2} during respiratory cycles. The circles and triangles are mixed venous and arterial P_{CO_2} recorded from *in vivo* studies.[30 31] (B) Dynamic $P_{E'CO_2}$ changes with different combinations of tidal volume and respiratory rate. The dots are $P_{E'CO_2}$ recorded from the patient and the solid line is the model prediction. (C) Effects of tidal volume and respiratory rate on the measured and predicted Pa_{CO_2} and $P_{E'CO_2}$. The carbon dioxide values predicted by the model closely follow those recorded in the patients. RR and V_T are respiratory rate and tidal volume respectively.

are the same as shown in Table 1. Both arterial and alveolar P_{CO_2} fluctuate during the respiratory cycle but arterial P_{CO_2} lags alveolar P_{CO_2}. Also demonstrated is that alveolar P_{CO_2} peaks shortly after the end of expiration. The average mixed venous and arterial P_{CO_2} are in agreement with the literature.[30 31]

Figure A2B shows the dynamic change of measured and predicted $P_{E'CO_2}$ following changes in tidal volume and frequency. After ethics committee approval and informed consent from the patient, a 59-yr-old 77-kg male patient undergoing vascular surgery was studied. The tidal volume and respiratory rate were set to: 950 and 15; 750 and 7; 500

and 6; 850 ml and 10 bpm respectively and in sequence. The $P_{E'CO_2}$ was recorded for each expiration. The model was set to simulate a 75-kg male subject undergoing mechanical ventilation with the same combinations of tidal volume and respiratory rate. The results show that the model simulation closely represents the dynamic change of $P_{E'CO_2}$ recorded from the patient (Fig. A2B).

Figure A2C shows the model's prediction of P_{aCO_2} and $P_{E'CO_2}$ and comparison with a published study.[32] In that study, 12 patients were ventilated with tidal volumes of 10, 7.5, 5 and 2.5 ml kg^{-1} and respiratory rates of 10, 13, 21 and 40 bpm respectively. Each setting was maintained for 10 min and P_{aCO_2} and $P_{E'CO_2}$ were measured and recorded.[32] The model was set to simulate a 75-kg male subject ventilated with the same tidal volumes and respiratory rates as the patients. Other parameters are the same as in Table 1. The anatomical dead-space was adjusted as a function of tidal volume.[33] At each setting, the model was run for 10 min and the P_{aCO_2} and $P_{E'CO_2}$ were recorded.[32] The average absolute error of the model predictions was 0.94% of the mean and 9.1% of the SD for measured P_{aCO_2}, and 4.4% of the mean and 28.4% of the SD for measured $P_{E'CO_2}$. This result is comparable with a model study by Hardman and Aitkenhead.[34]

Our results show that the model simulates realistically the gas exchange of a human lung both dynamically and in steady state.

Appendix C. Calculation of ventilation and perfusion to the three perfused and ventilated compartments in the model

In Part 3 of this study the ventilation and perfusion of the three ventilated and perfused alveolar compartments, $\dot{V}_1$, $\dot{V}_2$ and $\dot{V}_3$ and $\dot{V}_3$ and $\dot{Q}_1$, $\dot{Q}_2$ and $\dot{Q}_3$ litre min^{-1} respectively, were varied to simulate lungs with various degrees of $\dot{V}/\dot{Q}$ inhomogeneity. The $\dot{V}/\dot{Q}$ ratios of the ventilated and perfused compartments were fixed as follows:

$$\dot{V}/\dot{Q}=0.1 \quad (5)$$

$$\dot{V}/\dot{Q}=1 \quad (6)$$

$$\dot{V}/\dot{Q}=10 \quad (7)$$

The total ventilation $\dot{V}$, total perfusion $\dot{Q}$, shunt blood flow ($\dot{Q}_s$) and alveolar dead-space ventilation ($\dot{V}_{D_{alv}}$) were known, therefore:

$$\dot{V}_1+\dot{V}_2+\dot{V}_3+\dot{V}_{D_{alv}}=\dot{V} \quad (8)$$

$$\dot{Q}_1+\dot{Q}_2+\dot{Q}_3+\dot{Q}_s=\dot{Q} \quad (9)$$

There were six unknown parameters in five equations (Equations 5–9). We assigned values to $\dot{Q}_2$ and calculated the remaining five unknown parameters ($\dot{V}_1$, $\dot{V}_2$, $\dot{V}_3$, $\dot{Q}_1$ and $\dot{Q}_3$) by solving Equations 5–9 simultaneously. We used software written in Matlab (Mathworks, Natick, MA, USA) to solve the equations and hence determine the fractions of ventilation and perfusion directed to each alveolar compartment.

References

1 Wenzel U, Rudiger M, Wagner MH, Wauer RR. Utility of deadspace and capnometry measurements in determination of surfactant efficacy in surfactant-depleted lungs. *Crit Care Med* 1999; **27**: 946–52

2 Verschuren F, Liistro G, Coffeng R, *et al*. Volumetric capnography as a screening test for pulmonary embolism in the emergency department. *Chest* 2004; **125**: 841–50

3 Kline JA, Israel EG, Michelson EA, *et al*. Diagnostic accuracy of a bedside D-dimer assay and alveolar dead-space measurement for rapid exclusion of pulmonary embolism: a multicenter study. *JAMA* 2001; **285**: 761–8

4 Nuckton TJ, Alonso JA, Kallet RH, *et al*. Pulmonary dead-space fraction as a risk factor for death in the acute respiratory distress syndrome. *N Engl J Med* 2002; **346**: 1281–6

5 Hubble CL, Gentile MA, Tripp DS, *et al*. Deadspace to tidal volume ratio predicts successful extubation in infants and children. *Crit Care Med* 2000; **28**: 2034–40

6 Kars AH, Bogaard JM, Stijnen T, *et al*. Dead space and slope indices from the expiratory carbon dioxide tension-volume curve. *Eur Respir J* 1997; **10**: 1829–36

7 Bohr C. Ueber die Lungenathmung. *Skand Arch Physiol* 1891; **2**: 236–68

8 Enghoff H. Volumen inefficax, Bemerkungen zur Frage des schadlichen Raumes. *Upsala Lakareforen Forh* 1938; **44**: 191–218

9 Severinghaus JW, Stupfel M. Alveolar dead space. *Am J Physiol* 1955; **183**: 660

10 Fowler WS. Lung function studies. II: The respiratory dead space. *Am J Physiol* 1948; **154**: 405–16

11 Koulouris NG, Latsi P, Dimitroulis J, *et al*. Noninvasive measurement of mean alveolar carbon dioxide tension and Bohr's dead space during tidal breathing. *Eur Respir J* 2001; **17**: 1167–74

12 Fletcher R. Relationship between alveolar deadspace and arterial oxygenation in children with congenital cardiac disease. *Br J Anaesth* 1989; **62**: 168–76

13 Kuwabara S, Duncalf D. Effect of anatomic shunt on physiologic deadspace-to-tidal volume ratio–a new equation. *Anesthesiology* 1969; **31**: 575–7

14 Yem JS, Tang Y, Turner MJ, Baker AB. Sources of error in non-invasive pulmonary blood flow measurements by partial rebreathing: a computer model study. *Anesthesiology* 2003; **98**: 881–7

15 Weibel ER. *Morphometry of the Human Lung*, 3rd edn. Heidelberg: Springer, 1963

16 Gronlund J. Errors due to tissue CO_2 capacity in estimation of pulmonary blood flow from single-breath gas analysis. *Respir Physiol* 1983; **54**: 381–96

17 Olszowka AJ, Farhi LE. A system of digital computer subroutines for blood gas calculations. *Respir Physiol* 1968; **4**: 270–80

18 Farhi E, Rahn H. Dynamic changes in carbon dioxide stores. *Anesthesiology* 1960; **21**: 604–14

19 Cherniack NS, Longobardo GS. Oxygen and carbon dioxide gas stores of the body. *Physiol Rev* 1970; **50**: 196–243

20 Wagner PD, Dantzker DR, Dueck R, Clausen JL, West JB. Ventilation-perfusion inequality in chronic obstructive pulmonary disease. *J Clin Invest* 1977; **59**: 203–16

21 Fletcher R, Jonson B, Cumming G, Brew J. The concept of dead-space with special reference to the single breath test for carbon dioxide. *Br J Anaesth* 1981; **53**: 77–88

22 Wenzel U, Wauer RR, Wagner MH, Schmalisch G. *In vitro* and *in vivo* assessment of the Ventrak 1550/Capnogard 1265 for single breath carbon dioxide analysis in neonates. *Br J Anaesth* 1999; **83**: 503–10

23 Olsson K, Jonson B, Olsson CG, Wollmer P. Diagnosis of pulmonary embolism by measurement of alveolar dead space. *J Intern Med* 1998; **244**: 199–207

24 Dubois AB, Britt AG, Fenn WO. Alveolar CO_2 during the respiratory cycle. *J Appl Physiol* 1952; **4**: 535–48

25 Jones NL, Robertson DG, Kane JW. Difference between end-tidal and arterial P_{CO_2} in exercise. *J Appl Physiol* 1979; **47**: 954–60

26 Shankar KB, Moseley H, Kumar Y, Vemula V. Arterial to end tidal carbon dioxide tension difference during caesarean section anaesthesia. *Anaesthesia* 1986; **41**: 698–702

27 Fletcher R, Jonson B. Deadspace and the single breath test for carbon dioxide during anaesthesia and artificial ventilation. Effects of tidal volume and frequency of respiration. *Br J Anaesth* 1984; **56**: 109–19

28 Conti G, Antonelli M, Navalesi P, *et al*. Noninvasive vs. conventional mechanical ventilation in patients with chronic obstructive pulmonary disease after failure of medical treatment in the ward: a randomized trial. *Intensive Care Med* 2002; **28**: 1701–7

29 Breen PH, Mazumdar B, Skinner SC. How does experimental pulmonary embolism decrease CO_2 elimination? *Respir Physiol* 1996; **105**: 217–24

30 Mertzlufft FO, Brandt L, Stanton-Hicks M, Dick W. Arterial and mixed venous blood gas status during apnoea of intubation–proof of the Christiansen-Douglas-Haldane effect *in vivo*. *Anaesth Intensive Care* 1989; **17**: 325–31

31 Lumb A, Nunn JF. *Nunn's Applied Respiratory Physiology*, 5th edn. Oxford: Butterworth-Heinemann, 2000

32 Liebenberg CS, Raw R, Lipman J, Moyes DG, Cleaton-Jones PE. Small tidal volume ventilation using a zero deadspace tracheal tube. *Br J Anaesth* 1999; **82**: 213–6

33 Crawford AB, Makowska M, Engel LA. Effect of tidal volume on ventilation maldistribution. *Respir Physiol* 1986; **66**: 11–25

34 Hardman JG, Aitkenhead AR. Validation of an original mathematical model of CO_2 elimination and dead space ventilation. *Anesth Analg* 2003; **97**: 1840–5